Optics Letters

Low-cost high integration IR polymer microlens array

Feng Liu,[1,3] Qing Yang,[2,3] Feng Chen,[1,3,*] Fan Zhang,[1,3] Hao Bian,[1,3] and Xun Hou[1]

[1]State Key Laboratory for Manufacturing System Engineering and Shaanxi Key Laboratory of Photonics Technology for Information, School of Electronics & Information Engineering, Xi'an Jiaotong University, Xi'an 710049, China
[2]School of Mechanical Engineering, Xi'an Jiaotong University, Xi'an 710049, China
[3]International Joint Research Laboratory for Micro/Nano Manufacturing and Measurement Technologies, Xi'an Jiaotong University, Xi'an 710049, China
*Corresponding author: chenfeng@mail.xjtu.edu.cn

Received 9 January 2019; revised 16 February 2019; accepted 19 February 2019; posted 22 February 2019 (Doc. ID 357240); published 21 March 2019

In this Letter, a low-cost refractive convex microlens array device based on infrared a polymer is fabricated by a nanoimprinting technique. The device integrates more than 4000 microlenslets within a footprint of 10 mm × 10 mm. The surface quality, spectral transmittance, imaging resolution, and surface damage threshold of the device have been fully characterized. The IR imaging and parallel laser inscription experiments confirm the remarkable optical performance of the fabricated device. Owing to the merits of high optical quality, low fluence lose, and simple fabrication, this device is promising in cutting-edge IR applications, such as IR imaging, laser fabrication, and so on.

https://doi.org/10.1364/OL.44.001600

IR optics are highly demanded in fast-growing applications, for instance, biomedical imaging [1–3], remote monitoring [4,5], high-capacity telecommunication [6], metrology [7,8], and so on. In these applications, the system integration [3], multichannel processing [9], and effective coupling [10] require compact, lightweight, and high-quality optics. The mostly used IR materials are silicon, germanium, sapphire, chalcogenide glasses, and the devices are usually made by complex and expensive techniques with poor inefficiency, such as ultraprecision mechanical cutting [11,12], semiconductor epitaxial growth [13], mask-assisted etching [14], vacuum melt-quenching [15], etc. Both the material and the manufacturing made the IR optics extremely expensive, and normally the procedures are time-consuming. For example, a silicon optics fabrication by single point diamond turning could takes hours for a single component; photolithography not only requires complicated procedures but also takes more time. The booming applications in the IR region strongly desire low-cost highly efficient IR optics, however, such optics has still rarely been reported. In this Letter, we demonstrate a near IR (NIR) polymer convex microlens array (MLA) device, which has the advantages of compactness, light weight, economical manufacturing, and perfect imaging ability. Such an NIR MLA is fabricated by a nanoimprinting technique, so the device could be massively replicated. The final fabricated device is close-packed by more than 4000 convex microlenslet subapertures within a footprint of 10 mm × 10 mm. The working band covers a wide region from 780 nm to 2.2 μm. The fully characterized device shows high surface quality, imaging performance, and potential applications in NIR imaging and parallel processing.

The NIR MLA fabrication starts from a hard concave mold, which is made by a highly efficient maskless femtosecond laser assisted chemical etching (FLWE) technique on a BK-7 optical glass substrate [16–18]. The glass is exposed to tightly focused femtosecond laser pulses with the photon implantation dose of 135 kJ/cm^2 per site; then the hexagonally arrayed ablation craters with a pitch of 150 μm are etched down and polished by a chemical etchant, and at last a hard concave MLA mold with a nanometer scale surface roughness is formed. A thermoplastic NIR poly(methyl methacrylate) (PMMA) plate (Mitsubishi Chemical ACRYPET VH PF079) with a refractive index of 1.49 in the NIR region, density of 1.19 g/cm^3, and thickness of 1 mm is chosen to replicate the convex MLA by a nanoimprinting technique. The Vicat softening point of this NIR PMMA material is 107°C, and the optimal molding temperature of 115°C is obtained from the tests under our processing condition. The predried (80°C, 4 h) NIR plate is sandwiched between the mold and a specular glass substrate; then the assembled module is mounted on a homemade thermal nanoimprinting platform and is heated with a temperature increment of 9°C/min. When the molding temperature is reached, a pressure of 87 kPa is vertically applied onto the module by a servo motor and is kept for 180 s; then the module is left to cool down in the ambient temperature. The replicated polymer MLA is demolded in the DI water, assisted by an ultrasonic bath. The thickness of the fabricated device is measured as 0.6 mm. The surface profile of the fabricated NIR MLA is observed by the scanning electron microscope (SEM) (HITACHI, FlexSEM 1000), as shown in Fig. 1(a); the pitch of the microlenslets is 150 μm; and the fill factor approaches 100%.

The cross-section profiles of the microlenslets are measured by the laser scanning confocal microscope (Olympus LEXT

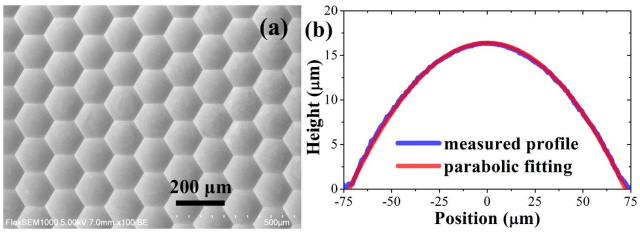

Fig. 1. (a) Surface profile of the NIR MLA device. (b) The measured transverse profile of the microlenslets, with the parabolic fitting for the measured data.

OLS4000). The sampled profiles show great uniformity and high surface quality, as shown in Fig. 1(b). The sag height is measured as 16 μm, and the surface roughness is estimated as 70 nm, i.e., $\lambda/15$. The measured data are well fitted by a parabolic function as $h = -0.00315 \times x^2 + 16.4$, where h is the height, x is the transverse position, and the units are in micrometers. The focal length of the device is measured as 380 μm, and the numerical aperture (NA) value of the microlenslet is calculated as 0.4.

The transmittance of the fabricated MLA has been measured by an UV-VIS-NIR spectrophotometer (Shimadzu UV-3600) with an integrating sphere detector, as shown in Fig. 2. The device shows relatively high transmittance in the whole NIR region due to its low absorption and low refractive index. Especially, it shows remarkable transparency in the typical NIR windows, such as 1030 nm for Yb^+-based lasers, 1064 nm for Nd:YAG lasers, 1550 nm for Er^+-doped fiber lasers, and 980 nm/1310 nm for InGaAs semiconductor lasers, and this may predict the application potential of the device in the NIR region.

The imaging performance has been evaluated by a quantitative test. The modulation transfer function (MTF) [19] of the imaging subaperture is calculated from the measured point spread function (PSF). The PSF of the device is measured by the system shown in Fig. 3(a). A microscope (Nikon ECLOPSE LV100ND) equipped with NIR objectives (Mitutoyo Plan Apo NIR, 20 × /NA0.40) and IR illumination source is used as the testing platform. A pinhole (Thorlabs, P100D) with a diameter of 100 μm was placed at the object plan of the collimator lens of Köhler illumination, and the MLA on the XY stage is illuminated by the collimated beam. The foci of the subapertures are magnified by a 20× NIR objective and relayed by a tube lens (omitted in the figure). They are then sampled by a TE-cooled InGaAs PIN-photodiode array sensor (Raptor photonics, OWL SW1.7 CL HS) with sensitive wavelength from 0.4 to 1.7 μm, dimension of 320 × 256, and pixel size of 30 μm. The sampled PSF of one single microlenslet is shown in Fig. 3(b). The foci array by the plane wave illumination is measured with intensity

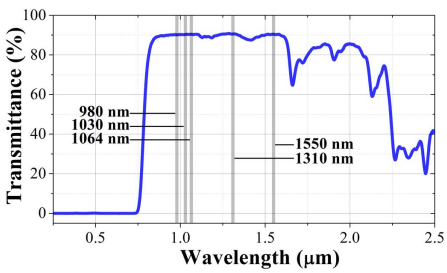

Fig. 2. Measured transmittance of the NIR MLA device.

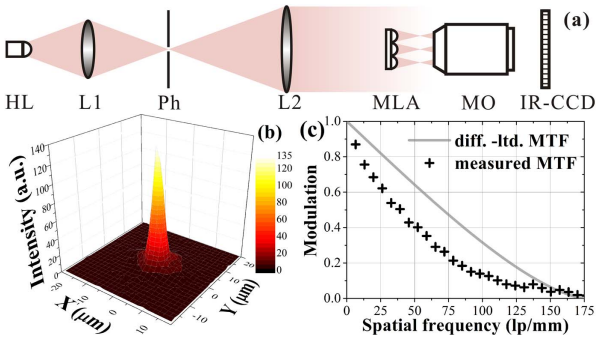

Fig. 3. (a) Schematic of PSF measurement setup for microoptics, in which the HL is the halogen lamp, L1 is the collector lens, Ph is the pinhole, L2 is the collimator lens, MLA is the sample device, MO is the microscope objective, and the IR-CCD is the imaging sensor working in the NIR region. (b) The measured PSF of one microlenslet. (c) The calculated MTF.

and pitch variations of 4% and 0.9%, respectively, indicating the good uniformity of the integrated device. The MTF is calculated by Fourier transform of the PSF, as shown in Fig. 3(c), and the modulation of imaging sensor is already corrected.

A positive USAF1951 resolution target (Daheng Corp., GCG-0206) is also imaged by the device to confirm its resolution performance. As shown in Fig. 4, the Group 6, Element 3 could be well recognized, indicating the resolving ability of 80.6 l p/mm, which meets the result in the MTF test well.

The fabricated MLA has been confirmed as a competitively arrayed NIR imaging device by the test shown in Fig. 5. A tungsten lamp (Philip, LV-HL50W) was chosen as an imaging target. In Figs. 5(a) and 5(c), the passive images are taken when the lamp is switched off, clearly showing the lamp structure. When the current (0.63 A at 0.9 V) is applied onto the lamp, the heated filament radiates wide IR rays. Clear IR images, as shown in Figs. 5(b) and 5(d), are captured when the background illumination is off, and the ambient light is shielded. The filament with a thickness of 0.1 mm could be well recognized in the zoomed IR image.

The NIR MLA device shows great optical performance, and it is potentially qualified in a parallel IR laser inscription. The laser-induced damage threshold (LIDT) of the device is first tested by the damage-probability statistics method [20,21]. Femtosecond laser pulses from a Yb^+-doped fiber amplifier (Amplitude system, SATSUMA HP2) with a central wavelength of 1030 nm and a pulse duration of 350 fs are focused to a 1.6 μm spot by a 20 × /NA0.40 objective and project onto

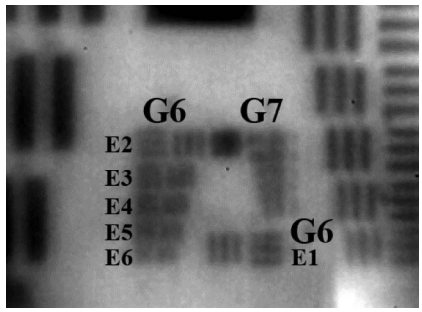

Fig. 4. NIR images of a standard USAF1951 resolution target plate sampled by the MLA.

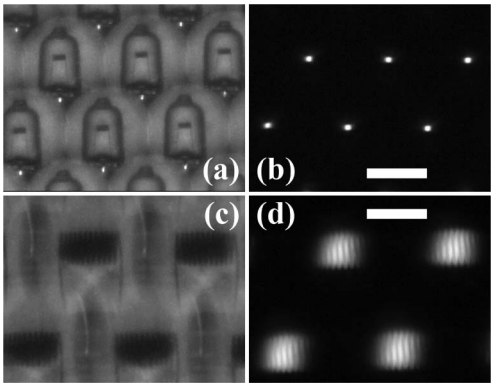

Fig. 5. NIR images of a tungsten lamp sampled by the MLA. (a) and (b) are captured by a 10× objective with the same scale bar of 10 mm. (c) and (d) are zoomed by a 20× objective with the same scale bar of 3 mm. Both the scale bars indicate the real size of the target.

the molded polymer plate surface. Both single pulse per site (1-on-1) and multishot per site (S-on-1, $S = 500$) cases are tested, as shown in Fig. 6(a). In the single pulse case, accompanying the increased incident fluence, laser pulses induce regional refractive index modification [22], micron scale surface deformation [23], and then direct ablation, and the LIDT is estimated as 2.0 J/cm^2. In the S-on-1 case, the accumulated thermal effects cause permanent material modification and induce lower LIDT, estimated as 0.7 J/cm^2.

A parallel laser inscription experiment is carried out, as shown in Fig. 6(b), to demonstrate the focusing power and the potential application of the device. The laser pulse train with average power of 1.9 W, repetition rate of 100 kHz, and beam width of 1.6 mm illuminates the MLA device, which only reaches 2‰ of its LIDT. The foci array is formed behind the device, and the focal spot size is 3.1 μm each, offering the fluence of 2.1 J/cm^2, which already exceeds the LIDT of the target polymer plate. An arrayed inscription pattern of capital letter "S" is formed by moving the target sample mounted on a 2D motorized translation stage with the speed of 50 μm/mm. All the inscription units perfectly reproduce the sample movement, and the width of the lines is 5 μm. With these results, the NIR MLA shows its capability as a high throughput microfabrication device.

In conclusion, a close-packed convex polymer MLA device with minimized volume and high transparency in the NIR region has been fabricated with an economical nanoimprinting technique. The replications have relatively good topography and surface quality. The quantitative evaluation and imaging test show excellent optical performance. The LIDT test shows the tolerance of the device in high laser fluence, and a highly efficient parallel laser inscription experiment confirms the strong focusing ability of the device. All the evidence shows the fabricated NIR MLA to be a competitive device for cutting-edge IR imaging and mass laser processing.

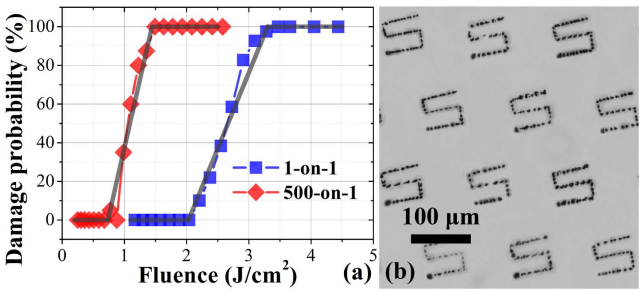

Fig. 6. (a) Relationship of the laser ablation probability and the incident fluence; the data in the changing region is linear fitted (solid gray line) to determine the damage threshold. (b) The laser microinscription pattern by the MLA device.

Funding. National Key Research and Development Program of China (2017YFB1104700); National Natural Science Foundation of China (NSFC) (51335008, 61435005, 61875158, U1630111); China Postdoctoral Science Foundation (2018M633499).

Acknowledgment. The authors thank the Collaborative Innovation Center of Suzhou Nano Science and Technology, and Instrument Analysis Center of Xi'an Jiaotong University. The SEM work was done at International Center for Dielectric Research (ICDR), Xi'an Jiaotong University.

REFERENCES

1. D. Borycki, O. Kholiqov, and V. J. Srinivasan, Opt. Lett. **42**, 591 (2017).
2. P. Si, E. Yuan, O. Liba, Y. Winetraub, S. Yousefi, E. D. SoRelle, D. W. Yecies, R. Dutta, and A. de la Zerda, ACS Nano **12**, 11986 (2018).
3. J. Wang, H. Li, G. Tian, Y. Deng, Q. Liu, and L. Fu, Biomed. Opt. Express **9**, 5011 (2018).
4. L. Tombez, E. J. Zhang, J. S. Orcutt, S. Kamlapurkar, and W. M. J. Green, Optica **4**, 1322 (2017).
5. C. B. Pereira, X. Yu, M. Czaplik, R. Rossaint, V. Blazek, and S. Leonhardt, Biomed. Opt. Express **6**, 4378 (2015).
6. K. Wang, A. Nirmalathas, C. Lim, E. Wong, K. Alameh, H. Li, and E. Skafidas, Opt. Lett. **43**, 3132 (2018).
7. A. Schliesser, N. Picqué, and T. W. Hänsch, Nat. Photonics **6**, 440 (2012).
8. A. Rolland, P. Li, N. Kuse, J. Jiang, M. Cassinerio, C. Langrock, and M. E. Fermann, Optica **5**, 1070 (2018).
9. Y. Zhao, W. R. Burger, M. Zhou, E. B. Bernhardt, P. A. Kaufman, R. R. Patel, C. V. Angeles, B. W. Pogue, K. D. Paulsen, and S. Jiang, Biomed. Opt. Express **8**, 4217 (2017).
10. W. Song, L. Zhou, S. Zhang, S. Ness, M. Desai, and J. Yi, Biomed. Opt. Express **9**, 3464 (2018).
11. Z. Sun, S. To, and K. M. Yu, Opt. Express **26**, 28161 (2018).
12. M. Mukaida and J. Yan, Int. J. Mach. Tools Manuf. **115**, 2 (2017).
13. I. Roland, Y. Zeng, X. Checoury, M. El Kurdi, S. Sauvage, C. Brimont, T. Guillet, B. Gayral, M. Gromovyi, J. Y. Duboz, F. Semond, M. P. de Micheli, and P. Boucaud, Opt. Express **24**, 9602 (2016).
14. J. Albero, L. Nieradko, C. Gorecki, H. Ottevaere, V. Gomez, H. Thienpont, J. Pietarinen, B. Päivänranta, and N. Passilly, Opt. Express **17**, 6283 (2009).
15. Y. Wang, S. Qi, Z. Yang, R. Wang, A. Yang, and P. Lucas, J. Non-Cryst. Solids **459**, 88 (2017).
16. F. Chen, Z. Deng, Q. Yang, H. Bian, G. Du, J. Si, and X. Hou, Opt. Lett. **39**, 606 (2014).
17. H. Bian, H. Liu, F. Chen, Q. Yang, P. Qu, G. Du, J. Si, X. Wang, and X. Hou, Opt. Express **20**, 12939 (2012).
18. F. Chen, H. Liu, Q. Yang, X. Wang, C. Hou, H. Bian, W. Liang, J. Si, and X. Hou, Opt. Express **18**, 20334 (2010).
19. A. Brückner, J. Duparré, R. Leitel, P. Dannberg, A. Bräuer, and A. Tünnermann, Opt. Express **18**, 24379 (2010).
20. "Lasers and laser-related equipment," ISO 21254-2:2011 (2011).
21. A. Žukauskas, G. Batavičiūtė, M. Ščiuka, T. Jukna, A. Melninkaitis, and M. Malinauskas, Opt. Mater. Express **4**, 1601 (2014).
22. C. Zheng, A. Hu, R. Li, D. Bridges, and T. Chen, Opt. Express **23**, 17584 (2015).
23. Y. Ou, Q. Yang, F. Chen, Z. Deng, G. Du, J. Wang, H. Bian, J. Yong, and X. Hou, IEEE Photon. Technol. Lett. **27**, 2253 (2015).